

AD-A009 867

CERAMIC SINTERING

Charles D. Greskovich, e. al

General Electric Corporate Research and Development

Prepared for:

Office of Naval Research  
Advanced Research Projects Agency

April 1975

DISTRIBUTED BY:

**NTIS**

National Technical Information Service  
U. S. DEPARTMENT OF COMMERCE

UNCLASSIFIED

SECURITY CLASSIFICATION OF THIS PAGE (When Data Entered)

REPORT DOCUMENTATION PAGE		READ INSTRUCTIONS BEFORE COMPLETING FORM
1. REPORT NUMBER	2. GOVT ACCESSION NO.	3. RECIPIENT'S CATALOG NUMBER <i>AD-A009 867</i>
4. TITLE (and Subtitle)  CERAMIC SINTERING		5. TYPE OF REPORT & PERIOD COVERED Semi-Annual Technical Rept. 11/1/74 to 4/30/75
		6. PERFORMING ORG. REPORT NUMBER SRD-75-047
7. AUTHOR(s) Charles D. Greskovich Joseph H. Rosolowski		8. CONTRACT OR GRANT NUMBER(s) N00014-74-C-0331
		10. PROGRAM ELEMENT, PROJECT, TASK AREA & WORK UNIT NUMBERS ARPA Order No. 2698 Program Code No. 4D10
9. PERFORMING ORGANIZATION NAME AND ADDRESS General Electric Company Corporate Research and Development Schenectady, New York 12301		12. REPORT DATE April 1975
		13. NUMBER OF PAGES <i>62</i>
11. CONTROLLING OFFICE NAME AND ADDRESS Advanced Research Projects Agency 1400 Wilson Blvd. Arlington, Virginia 22217		15. SECURITY CLASS. (of this report) Unclassified
		15a. DECLASSIFICATION/DOWNGRADING SCHEDULE
14. MONITORING AGENCY NAME & ADDRESS (if different from Controlling Office) Office of Naval Research 800 North Quincy St. Arlington, Virginia 22217		
16. DISTRIBUTION STATEMENT (of this Report)  APPROVED FOR PUBLIC RELEASE; DISTRIBUTION UNLIMITED		
17. DISTRIBUTION STATEMENT (of the abstract entered in Block 20, if different from Report)		
18. SUPPLEMENTARY NOTES		
19. KEY WORDS (Continue on reverse side if necessary and identify by block number)  Sintering, Silicon Carbide, Silicon		
20. ABSTRACT (Continue on reverse side if necessary and identify by block number)  Microstructure development during the sintering of densifying and non-densifying powders of $\beta$ -SiC was observed. The kinetics of grain growth and porosity decrease in the densifying powders, as well as the microstructure development, were found to be very similar to those observed in oxide powders. On sintering, the non-densifying powders developed a structure consisting of mutually interconnected, highly dense clusters of 50-100 grains separated by (continued on reverse side)		

DDC  
RECEIVED  
MAY 21 1975  
RECEIVED  
B

DD FORM 1473 JAN 73

EDI

Reproduced by  
NATIONAL TECHNICAL  
INFORMATION SERVICE  
US Department of Commerce  
Springfield, VA. 22151

UNCLASSIFIED  
SECURITY CLASSIFICATION OF THIS PAGE (When Data Entered)

PRICES SUBJECT TO CHANGE

20.

large, interconnected pores. It is concluded that the absence of shrinkage during sintering of a powder compact is not due to an intrinsic inability of the powder particles to agglomerate into dense clusters of grains, but probably rather to the disappearance of high energy grain boundaries during the course of the development of the small, dense regions observed in the microstructure. Sintered, non-densifying Si powders were found to have very similar microstructures to those observed in  $\beta$ -SiC. A Si powder of  $\sim 600\text{\AA}$  particle size was found to sinter to 92% theoretical density without the addition of dopants as sintering aids. It was found that the resistivity of B containing, dense sintered  $\beta$ -SiC could be changed through compensation of the B acceptors by N donors introduced from the sintering furnace atmosphere during firing. The thermal EMF of a junction made of p and n types of dense, sintered  $\beta$ -SiC was measured over the temperature range from 100°C to 1500°C.

TABLE OF CONTENTS

	<u>Page</u>
FOREWORD . . . . .	iv
SUMMARY . . . . .	v
LIST OF ILLUSTRATIONS . . . . .	viii
LIST OF TABLES . . . . .	xi
I. Introduction . . . . .	1
II. Grain Growth and Densification in $\beta$ -SiC Containing Boron and Carbon . . . . .	1
III. Dihedral Angles in Sintered $\beta$ -SiC . . . . .	14
IV. Development and Shrinkage of Grain Boundaries in Sintered $\beta$ -SiC Containing 0.8 wt% C . . . . .	21
V. Sintering of Silicon . . . . .	27
VI. Properties of Doped, Dense, Sintered $\beta$ -SiC . . . . .	42
REFERENCES . . . . .	49

## FOREWORD

This research was sponsored by the Advanced Research Projects Agency and carried out in the Physical Chemistry Laboratory of the General Electric Corporate Research and Development Center under U.S. Navy Contract N00014-74-C-0331 entitled "Ceramic Sintering".

The work was performed during the period November 1, 1974 to April 30, 1975.

The authors gratefully acknowledge the ceramic processing skill of Mr. C. Bobik and Mr. C. O'Clair. Dr. S. Prochazka did the work on the resistivity and thermal EMF of sintered  $\beta$ -SiC.

## SUMMARY

The work in this contract period was primarily directed to making observations on the development of microstructure during the sintering of doped and undoped  $\beta$ -SiC and Si. The objective was to elucidate the reasons why pure powders of covalent solids normally do not densify during sintering and how those dopants and powder preparation techniques that enable  $\beta$ -SiC to be sintered to densities greater than 96% operate. The hope is that this knowledge will guide the successful development of techniques for densifying powders of other technologically useful phase-pure covalent solids, such as AlN and Si<sub>3</sub>N<sub>4</sub>, by sintering.

Measurements of density and relative grain size in bodies formed by sintering a  $\beta$ -SiC powder containing 0.8 wt% C and 0.6 wt% B for 1 hr at various temperatures between 1500°C and 2050°C were made. These show that for this powder, which can be sintered to 95+% of theoretical density, the grain growth and sintering kinetics are very similar to those observed when sintering oxide powders. The sintering behavior of this powder is therefore not atypical. An activation energy for grain growth of 80 Kcal/mol was obtained from these measurements.

Densification of a  $\beta$ -SiC powder will stop if large single crystal plates of  $\alpha$ -SiC form in the sintering body. These large plates contact each other and form an effectively rigid framework which prevents the further shrinkage of the body.

Examination of the microstructures developed when nondensifying powders of  $\beta$ -SiC are fired reveals that a great deal of densification occurs on a microscopic scale. The structure is composed of apparently pore-free polycrystalline regions connected to similar regions at a few points with a separating, interconnected structure of large pores. The dense regions are typically composed of 50-100 grains and formed from the coalescence of several thousand of the original, fine powder

particles. Thus sintering to near theoretical density occurs on a microscopic scale (but still large in terms of the number of powder particles involved) but the densification does not extend throughout the body, so little or no shrinkage results. The dihedral angles observed at the pore-grain boundary intersections in this structure were all around  $100^\circ$  or greater; i.e., much larger than the minimum value of  $60^\circ$  required for pore closure, hence complete densification, to occur.

A nondensifying powder of  $\beta$ -SiC was hot-pressed at  $2050^\circ\text{C}$  to force partial densification (79%) and the development of many interparticle necks, each of which normally contains a grain boundary. This sample was then annealed at  $150^\circ\text{C}$  below the hot-pressing temperature in the absence of pressure. Except for a difference in the scale of grain size, the structure of the hot-pressed and annealed sample was identical to that of a sample which had only been sintered at  $1900^\circ\text{C}$ . The considerable amount of pore and grain growth that occurred during the annealing treatment indicated the instability of the hot-pressed, low density structure arising possibly from the presence of high energy grain boundaries. The shrinkage of these boundaries under the influence of tensile stresses, which arise when local densification occurs and which leads to the eventual separation of grains, could account for the observed course of microstructure development. The question that remains is why this mechanism does not prevent the development of the dense regions which are composed of a large number of grains.

Experiments performed with nondensifying powders of Si show that microstructures develop on sintering which are similar in all characteristics with those observed with  $\beta$ -SiC. This implies that the nonsinterability characteristic arises from the same causes in both materials. These Si powders could be made to shrink a small amount ( $\sim 4\%$ ) during sintering by the addition of 0.2 wt% C + 1.2 wt% B, but the little shrinkage that occurred seemed to depend principally on having a small average particle size. This was  $0.23 \mu$  for the

finest of these powders. A powder which was made by the thermal decomposition of silane and which had an average particle size of  $\sim 600 \text{ \AA}$  readily sintered to 92% of theoretical density without the use of additives. Thus, Si, too, is not intrinsically unsinterable.

In line with the contract objective of measuring properties of potential technological importance on dense bodies of covalently bonded ceramics prepared by sintering, experiments were performed to determine the electrical resistivity of dense, sintered  $\beta$ -SiC containing B dopant as a sintering aid. The objective was to determine if the normally p type conductivity introduced by this dopant could be compensated by N introduced from the furnace atmosphere during sintering. The results showed that both n and p type conductivity could be produced in the ceramic, as well as a range of conductivity values, depending on the composition of the furnace atmosphere. A thermocouple was made of a junction of n and p type sintered  $\beta$ -SiC. With a cold junction temperature of  $100^\circ\text{C}$ , the thermal EMF of the hot junction was found to be 0.95 volt at  $1500^\circ\text{C}$  and 0.25 volt at  $500^\circ\text{C}$ .

LIST OF ILLUSTRATIONS

<u>Fig. No.</u>		<u>Page</u>
1	Relative density and grain size as a function of sintering temperature for Powder I . . . . .	5
2	Cubic grain growth rate constant versus reciprocal temperature for Powder I . . . . .	5
3	SEM photomicrographs of fractured surfaces of sintered specimens of Powder I ( $\beta$ -SiC + 0.8% C + 0.6% B) heat treated at 2000°C for A) 2 min, B) 10 min, C) 60 min, and D) 300 min. X10,000 . . . . .	7
4	Relative density versus logarithm of time for Powder I ( $\beta$ -SiC + 0.8 wt% C + 0.6% B) sintered at 2000°C in argon . . . . .	8
5	Polished section of a specimen of Powder I ( $\beta$ -SiC + 0.8% C + 0.6% B) sintered for 300 min at 2000°C. Note large dense regions in the microstructure. X150 . . . . .	9
6	Microstructure of a dense, solid region in sintered $\beta$ -SiC containing 0.8% C and 0.6% B. Chemically etched in 10 parts KOH + 1 part KNO <sub>3</sub> at 650°C for 30 seconds. X1000 . . . . .	10
7	SEM photographs of fractured surfaces of specimens of Powder II ( $\beta$ -SiC + 0.7% C + 1% B <sub>4</sub> C) sintered for 1 hr in argon at A) 1700°C, B) 1900°C and C) 2100°C. Note long plates of $\alpha$ -SiC in B) and C). X2000 . . . . .	13
8	TEM photomicrograph of sintered particles of loose powder of $\beta$ -SiC containing 0.8% C fired at 1900°C for 1 hr in argon. X40,000 . . . . .	16
9	TEM photograph of a group of sintered particles of $\beta$ -SiC. Sintered at 1900°C for 1 hr in argon. X100,000 . . . . .	17
10	Five-sided pore in the microstructure of a powder compact of $\beta$ -SiC containing 0.8% C that was sintered at 1900°C for 1 hr in argon. X150,000 . . . . .	18

(LIST OF ILLUSTRATIONS - cont.)

<u>Fig. No.</u>		<u>Page</u>
11	Microstructure of hot-pressed $\beta$ -SiC containing 0.8% C which was subsequently annealed at 1900°C for 2 hrs in argon. X2000 . . . . .	19
12	Sintered particles of loose powder of $\beta$ -SiC containing 0.6% B fired at 1900°C for 2 hrs in argon. X100,000 . . . . .	20
13	Sintered particles of loose powder of $\beta$ -SiC containing 0.8% C and 0.6% B fired at 1900°C for 2 hrs in argon. X100,000 . . . . .	22
14	SEM photomicrographs of a fractured surface of A) a "green" compact and B) sintered compact (1900°C-1 hr-Ar) of $\beta$ -SiC powder containing 0.8% C. . . . .	23
15	Microstructure of a sintered specimen of $\beta$ -SiC containing 0.8% C fired at 1900°C for 1 hr in argon. SEM of fractured surface. X2000 . . . . .	25
16	Microstructure of a hot-pressed specimen of $\beta$ -SiC powder containing 0.8% C. Specimen was hot-pressed at 10,000 psi for 1 hr at 2050°C. SEM of fractured surface. X2000 . . . . .	25
17	Microstructure of hot-pressed $\beta$ -SiC containing 0.8% C which was A) annealed at 1700°C and B) annealed at 1900°C for 2 hrs in argon. SEM of fractured surface. X2000 . . . . .	26
18	Microstructure of silicon containing 0.2% C and 1.2% B sintered to 99+% of theoretical density at 1391°C for 1 hr in argon. Reflected light photomicrograph of polished section. X500 . . . . .	32
19	SEM photomicrographs of fractured surfaces of A) a green compact of silicon before sintering, B) a sintered compact of silicon and C) a sintered compact of silicon containing 0.2% C and 1.2% B. Specimens B) and C) were sintered at 1350°C for 1 hr in Ar. X1000 . . . . .	34

(LIST OF ILLUSTRATIONS - cont.)

<u>Fig. No.</u>		<u>Page</u>
20	SEM photomicrograph of a fractured surface of silicon sintered at 1350°C for 1 hr in Ar. X5000 . . . . .	35
21	Reflected light micrograph showing polycrystalline nature of the solid, dense regions developed during the sintering of silicon at 1350°C for 1 hr in Ar. Polished section was chemically etched with mixture of equal parts of HF and HNO <sub>3</sub> at room temperature for 2 seconds. . . . .	36
22	Linear shrinkage as a function of specific surface area for silicon powders sintered at 1350°C for 1 hr in Ar. . . . .	41
23	Resistivity versus 1/T for variously doped hot-pressed, and sintered specimen of β-SiC . .	46
24	Thermal EMF of a junction of p and n types of β-SiC for: A) cold junction at 0°C, and B) cold junction at 100°C. . . . .	48

LIST OF TABLES

<u>Table No.</u>		<u>Page</u>
I	Characteristics of $\beta$ -SiC Powders I and II . . .	4
II	Comparison of Relative Density (D) and Specific Surface Area (S.A.) of Sintered Compacts of Powders I and II . . . . .	12
III	Effect of Particle Size and Composition on Density of Silicon Sintered at 1350°C for 1 hr in Ar . . . . .	30
IV	Specific Surface Area and Sintered Densities of Silicon Powders Prepared from Silane . . . .	39
V	Powder Characteristics and Sintering Behavior of Silicon . . . . .	40
VI	Effect of Sintering Furnace Atmosphere on the Resistivity of B-doped, Dense, Sintered $\beta$ -SiC . . . . .	44

## I. Introduction

The principal effort in the contract period reported here has been directed toward making observations on microstructure development during sintering of  $\beta$ -SiC and Si, both with and without dopants. This is a continuation of the work started in the first contract period and reported in the first Semi-Annual Technical Report<sup>(1)</sup>. The goal of this research program is the development of an understanding of the reasons why powders of covalently bonded solids are normally unsinterable. Emphasis is placed on advancing sintering theory as well as learning how to produce dense bodies of covalently bonded solids by conventional sintering. Sections II, III and IV of this report describe observations on grain growth and the behavior of grain boundaries and grain boundary-pore intersections during the sintering of  $\beta$ -SiC, both with and without the additives that enable this material to be sintered to near theoretical density.

Section V is devoted to describing the microstructures developed when powders of Si are sintered. This is one of several materials which will be investigated to determine the details of the microstructure development that are common to unsinterable (meaning non-densifying) powders.

It is also one of the tasks under this contract to make and report measurements of possible technological significance on any dense, covalently bonded ceramic which can be made by conventional sintering. Accordingly, in the first part of Section VI, we report measurements of resistivity of dense  $\beta$ -SiC ceramics containing several additives. In the second part of this Section we report measurements of the thermal EMF of a thermocouple junction made of p and n-type, dense, sintered  $\beta$ -SiC.

## II. Grain Growth and Densification in $\beta$ -SiC Containing Boron and Carbon

In an attempt to further understand the factors controlling the sintering of covalently bonded  $\beta$ -SiC, an investigation of grain

growth and densification was undertaken at high temperatures. These two processes are found to be interrelated during sintering of ionic and metallic powders, such as  $\text{Al}_2\text{O}_3$  and Cu, respectively, in a manner such that the activation energy is nearly the same for grain growth and densification. In the case of Cu, the experimentally observed activation energy for densification is about 46 Kcal/mole<sup>(2)</sup> and agrees well with the activation energy for volume self-diffusion in Cu<sup>(3)</sup>. An investigation of the atomic mobility in  $\beta$ -SiC doped with B and C was pursued through grain growth experiments.

Two types of  $\beta$ -SiC powders, containing both C and B, were investigated. These powders are designated as Powder I and Powder II, and are characterized in Table I. Early in the sintering of Powder II, large plate-shaped grains formed in the porous compacts and made it impossible to calculate a realistic value for the activation energy for grain growth. The sintering behavior of Powder II will therefore be discussed in the last part of this section.

#### A. Sintering behavior of Powder I

Disk-shaped powder compacts were formed by die-pressing 3 g samples in a 5/8" diameter die at 2500 psi followed by isostatic pressing at 30,000 psi to obtain green densities of about 59% of theoretical (the theoretical density of  $\beta$ -SiC is about 3.21 g/cc).

Sintering experiments were performed in flowing Ar ( $\sim 5$  ppm  $\text{O}_2$ ) at one atmosphere in a carbon element resistance furnace. Specimens were fired in a graphite crucible for 1 hr hold times at various temperatures from 1500°C to 2100°C. The effective oxygen pressure inside the furnace was not determined. Temperature was measured optically and controlled to  $\pm 20^\circ\text{C}$ . The apparent density of a sintered piece was calculated from its mass and volume. Grain size was determined from scanning electron micrographs of fractured

surfaces at magnifications of 10,000X by measuring approximately 50 to 100 grains in each specimen.

The results of the grain size and density measurements of the sintered specimens are given in Fig. 1 as a function of sintering temperature. Approximate error bars are shown on representative data points. The shapes of these curves are similar to those found for the sintering of  $\text{Al}_2\text{O}_3$  and other ionic materials. If it is assumed that a cubic grain growth law is obeyed, as is found during the sintering of most ionic materials, then an activation energy for grain growth can be calculated. Hence it is assumed that

$$d^3 - d_0^3 = k(t - t_0) \quad (1)$$

where  $d$  is the average grain size,  $d_0$  is the initial average grain or particle size,  $k$  is the temperature-dependent grain growth rate constant,  $t$  is time at temperature and  $t_0$  is the induction time for the beginning of grain growth. It is assumed that  $t \gg t_0$ . The grain growth rate constant is calculated at each temperature according to Eq. 1. By using the defining equation for  $k$ ,

$$k = k_0 \exp(-Q/RT) \quad (2)$$

where  $k_0$  is a constant,  $Q$  is the activation energy for grain growth and  $RT$  is thermal energy, the slope of the plot of  $\log k$  vs.  $1/T$  is equal to  $-Q/2.3R$ . Such a plot on semilogarithmic coordinates is shown in Fig. 2. The activation energy was calculated to be approximately 80 Kcal/mol. This magnitude of activation energy for grain growth in covalently bonded  $\beta$ -SiC containing 0.8 wt% C + 0.6% B is not unusual when compared to values obtained for oxides. In fact, this activation energy is lower than expected and is lower than those (150 Kcal/mol and 104 Kcal/mol, respectively) found for grain growth in  $\text{Al}_2\text{O}_3$ <sup>(4)</sup> and  $\text{BeO}$ <sup>(5)</sup>.

TABLE I  
Characterization of  $\beta$ -SiC Powders I and II

	POWDER I	POWDER II
<u>Method of preparation</u>	gas phase reaction in plasma torch	solid state reaction Si+C
<u>Composition</u>	$\beta$ -SiC+0.8 wt% C+0.6% B	$\beta$ -SiC+0.7 wt% C+1% B <sub>4</sub> C
<u>Specific surface area</u>	8 m <sup>2</sup> /g	11 m <sup>2</sup> /g
<u>Major impurities (ppm)</u>	O 1700, W 300, Fe 200, Cl 200	O 4400, Fe 270, Al 150

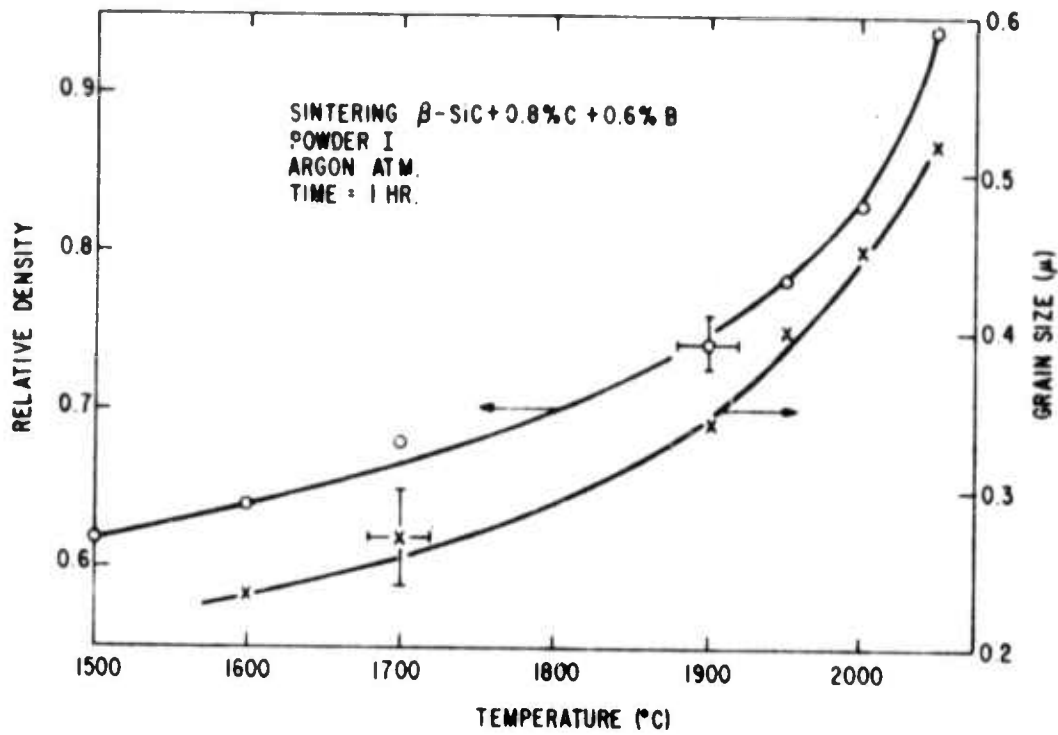


Fig. 1 Relative density and grain size as a function of sintering temperature for Powder I.

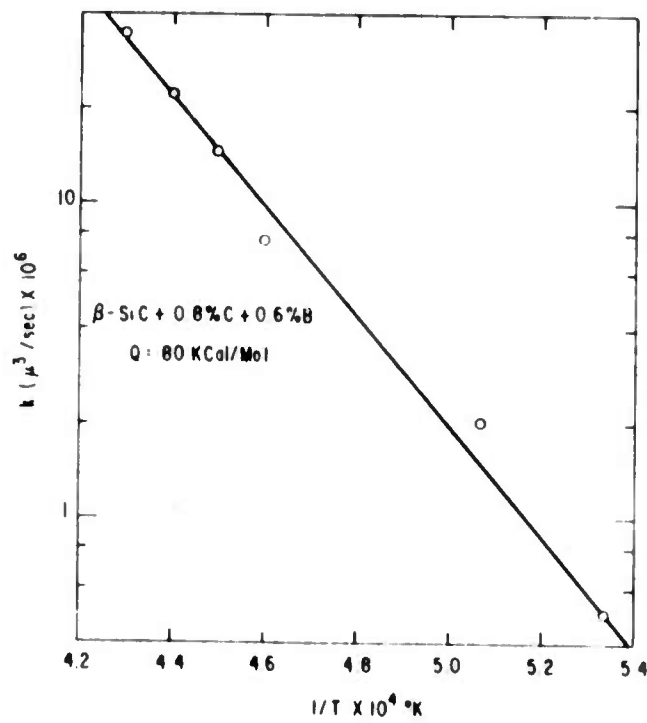
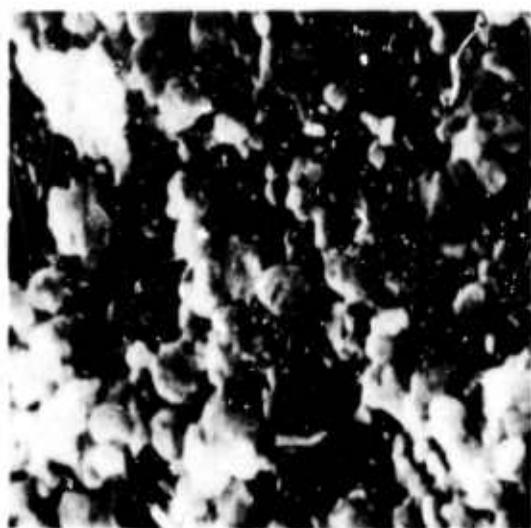


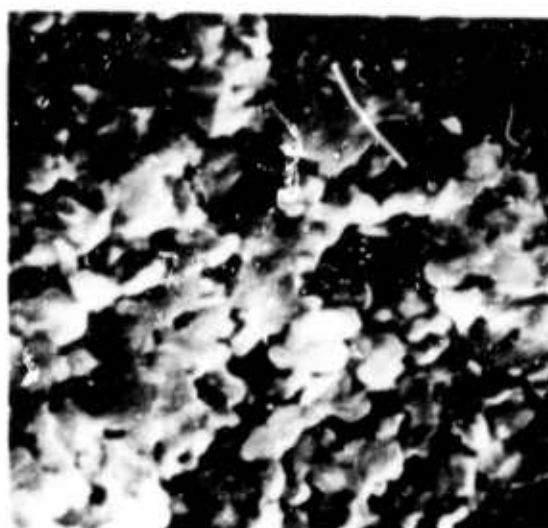
Fig. 2 Cubic grain growth rate constant versus reciprocal temperature for Powder I.

The kinetics of microstructural development at 2000°C was followed by SEM photomicrographs (Fig. 3) of fractured surfaces of the sintered specimens and by measuring density versus time (Fig. 4). It was hoped that grain growth kinetics could also be obtained from such photomicrographs. However, due to the small changes in grain size occurring with time at temperature, no reliable data could be obtained. A further complicating factor in determining the grain growth kinetics was the formation of large, dense, solid regions in the fine-grained matrix. This microstructure development is clearly shown in Fig. 3. A polished section of a sample sintered for 300 min at 2000°C is shown in Fig. 5. There is a large size distribution of "blocky" dense, solid regions which range from about 1 to 100  $\mu$  in the fine-grain ( $\sim 0.5 \mu$ )  $\beta$ -SiC matrix. A chemically etched, polished section reveals that these dense regions are polycrystalline (Fig. 6). The origin of these regions is believed to be associated with the size distribution of aggregates known to exist in this unprocessed,  $\beta$ -SiC powder. This speculation is supported by the fact that such "blocky", dense regions do not form during the sintering of the same powder if it receives a ball-milling treatment to comminute the particle aggregates. In order to fabricate sintered  $\beta$ -SiC articles having high strength, it is mandatory that the powder be processed to insure the development of a homogeneous, fine-grained microstructure.

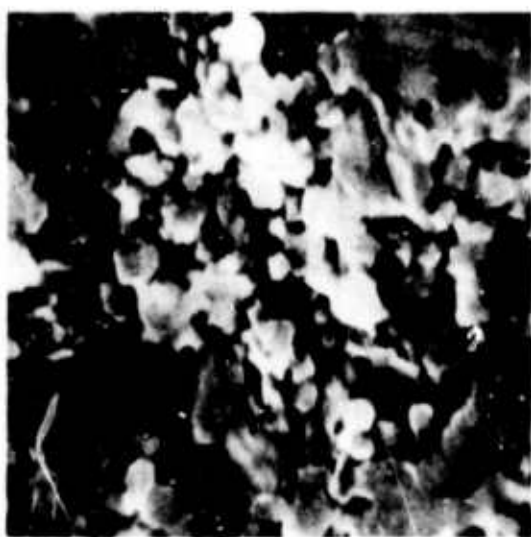
Figure 4 illustrates the linear relation between relative density and the logarithm of sintering time. This relationship is frequently found in the sintering of oxides and metals and, according to recent work<sup>(2)</sup>, can be understood on a theoretical basis if grain growth kinetics follow a cubic law. It, therefore, appears that the isothermal densification kinetics for covalently bonded  $\beta$ -SiC, doped with B and C, are not atypical.



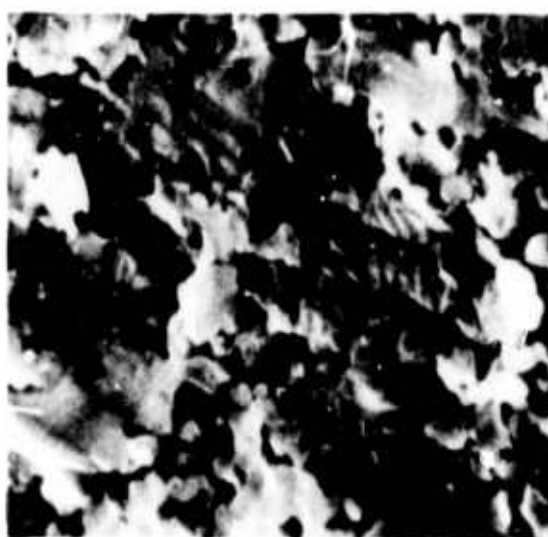
A



B



C



D

Fig. 3 SEM photomicrographs of fractured surfaces of sintered specimens of Powder I ( $\beta$ -SiC + 0.8% C + 0.6% B) heat treated at 2000°C for (A) 2 min, (B) 10 min, (C) 60 min, and (D) 300 min. 10,000X

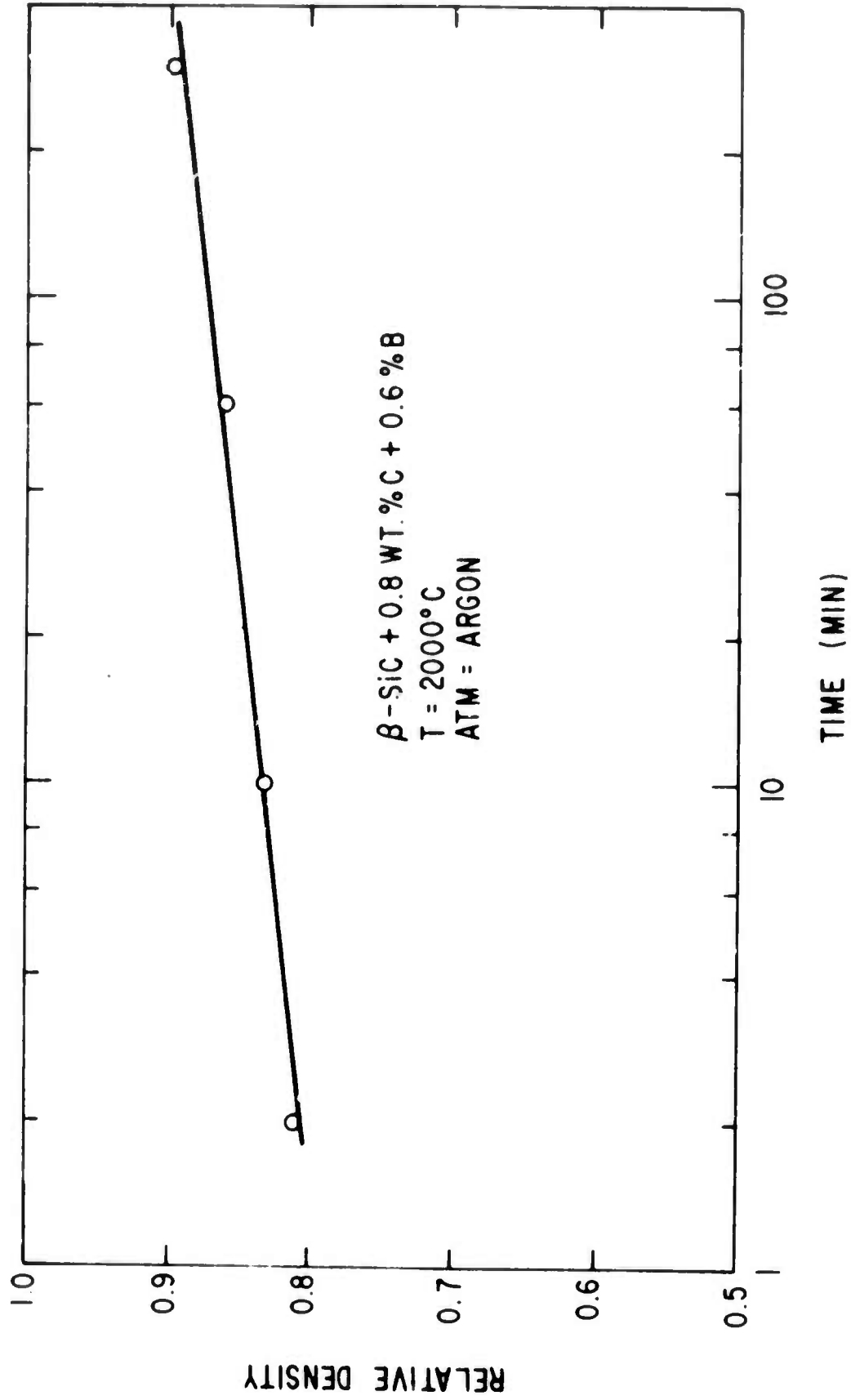


Fig. 4 Relative density versus logarithm of time for Powder I ( $\epsilon$ -SiC + 0.8 wt% C + 0.6% B) sintered at 2000°C in argon.

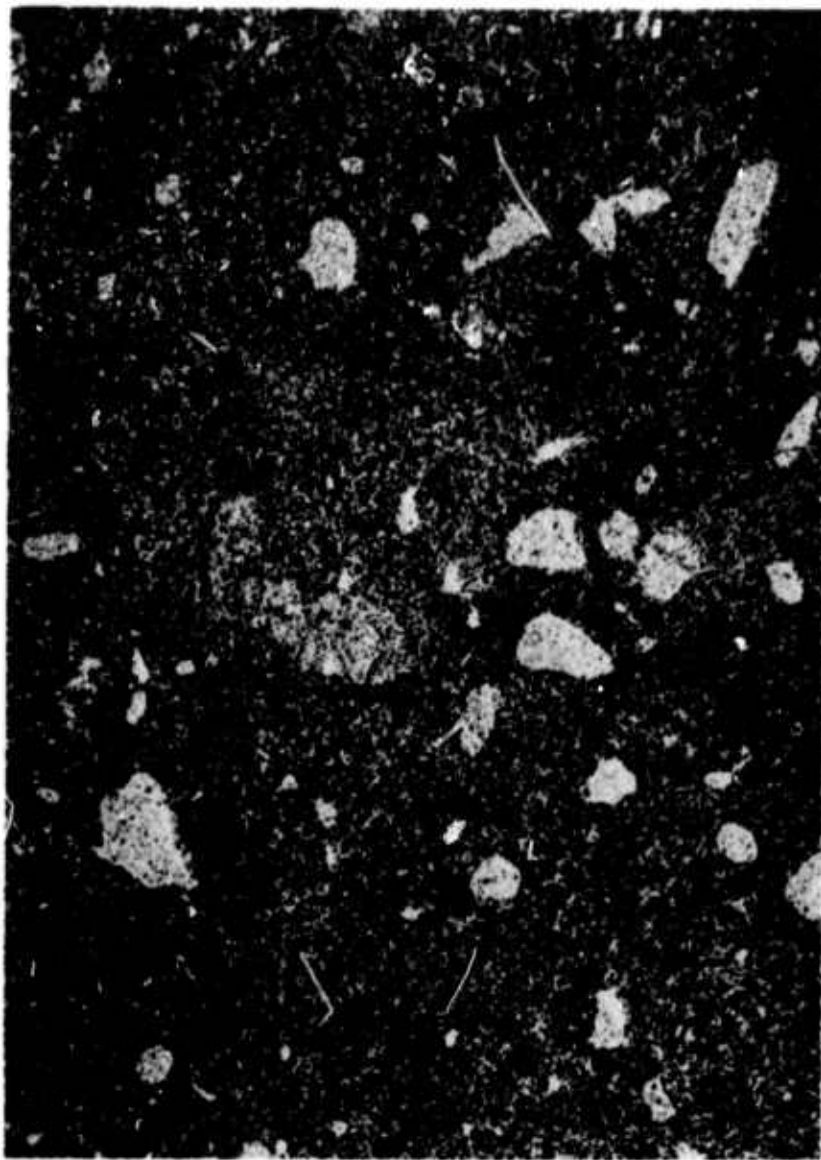


Fig. 5 Polished section of a specimen of Powder I ( $\beta$ -SiC + 0.8% C + 0.6% B) sintered for 300 min at 2000°C. Note large dense regions in the microstructure. 150X



Fig. 6 Microstructure of a dense, solid region in sintered  $\beta$ -SiC containing 0.8% C and 0.6% B. Chemically etched in 10 parts KOH + 1 part KNO<sub>3</sub> at 650°C for 30 seconds. 1000X

## B. Sintering behavior of Powder II

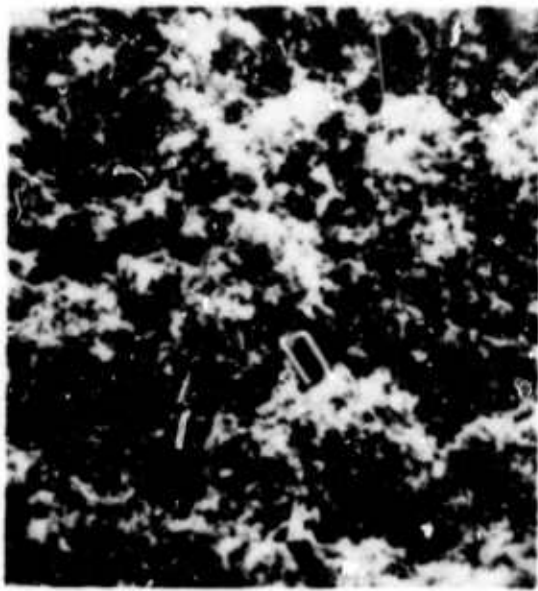
The characterization of Powder II is shown in Table I. This  $\beta$ -SiC powder was synthesized from the elements by a solid state reaction,  $\text{Si} + \text{C} \rightarrow \text{SiC}$ , and subsequently leached with  $\text{HF} + \text{HNO}_3$  to remove free Si, and then heated at  $< 600^\circ\text{C}$  in air to burn off free C. The specific surface area of the starting powder is not much different from that of Powder I. Addition of 0.5 to 0.8 wt% boron in the elemental form or as  $\text{B}_4\text{C}$  has been found to have the same effect on the sintering of Powder I<sup>(6)</sup>. Hence, the different sources of the boron in these two powders should not affect the sintering behavior. Finally, Powder I has only about 40% as much oxygen impurity as that found in Powder II.

The relative density and specific surface area of sintered compacts of Powder II are listed in Table II and compared with those measured for Powder I. It is interesting that compacts of Powder II exhibit  $\sim 17\%$  reduction in specific surface area after firing at  $1700^\circ\text{C}$  for 1 hr, but no densification. Compacts of Powder I, on the other hand, densify about 9% at  $1700^\circ\text{C}$  while the surface area reduces to about 25% of its original value. Densification of Powder II begins somewhere between 1700 and  $1900^\circ\text{C}$  and reaches a maximum value of 86% of theoretical at  $2100^\circ\text{C}$ . Prolonged sintering times and/or higher temperatures do not increase the density beyond 86%. By comparison, sintered samples of Powder I can be made with densities as high as 96% of theoretical by firing at  $2100^\circ\text{C}$ .

A question to be answered is why do sintered specimens of Powder II have a limiting density near 86%. Perhaps the answer can be found in SEM photomicrographs of fractured surfaces of specimens sintered at 1700, 1900 and  $2100^\circ\text{C}$  in argon for 1 hr (Fig. 7). The microstructure of the specimen sintered for 1 hr at  $1700^\circ\text{C}$  shows a very fine grain and pore structure. After 1 hr

TABLE II  
Comparison of Relative Density (D) and Specific  
 Surface Area (S.A.) of Sintered Compacts of Powders I and II

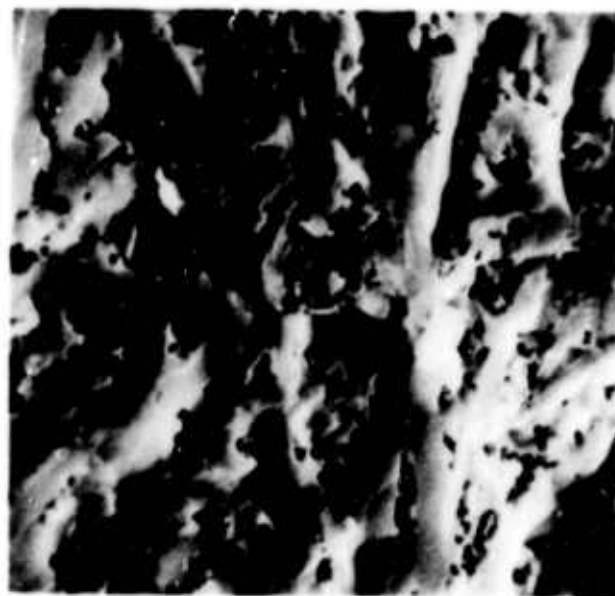
<u>Sintering conditions</u>	POWDER I		POWDER II	
	<u>D(%)</u>	<u>S.A. (m<sup>2</sup>/g)</u>	<u>D(%)</u>	<u>S.A. (m<sup>2</sup>/g)</u>
As pressed	59	8	53	11
1500-1 hr-Ar	60	8.5	53	11
1600 1 hr-Ar	64	7.8		
1700-1 hr-Ar	68	6	53	9.1
1900-1 hr-Ar	74	4	65	3.4
2100-1 hr-Ar	96		86	



A



B



C

**Fig. 7** SEM photographs of fractured surfaces of specimens of Powder II ( $\beta$ -SiC + 0.7% C + 1% B<sub>4</sub>C) sintered for 1 hr in argon at (A) 1700°C, (B) 1900°C, and (C) 2100°C. Note long plates of  $\alpha$ -SiC in (B) and (C). 2000X

of sintering at 1900°C, long thin plates have already developed in the fine-grained matrix of the sintered specimen which is only 54% dense. Dense plates as long as 20  $\mu$  and approximately 0.6 to 0.8  $\mu$  thick are visible in Fig. 7B. By increasing the sintering temperature to 2100°C (Fig. 7C), there is an increase in the length and number density of these dense plates. Furthermore, the average pore size appears to increase with increasing temperature (compare Figs. 7B and 7C). X-ray diffraction analysis has identified the plates as  $\alpha$ -SiC.

It is believed that the low terminal density of ~86% of theoretical is associated with the formation of large  $\alpha$ -SiC plates growing in the fine-grained  $\beta$ -SiC matrix. The large  $\alpha$ -SiC plates can reduce the shrinkage rate of the much finer (0.3  $\mu$ )  $\beta$ -SiC grains by a particle-size dilution effect. This type of effect is expected from sintering theory. A more important effect which strongly retards densification is the development of a continuous network of  $\alpha$ -SiC plates which acts to rigidize the sintering body (see Fig. 7C). Once the large  $\alpha$ -SiC plates impinge on one another to make a continuous framework throughout the structure, densification essentially ceases because the coordinated atomic adjustments at the grain boundaries necessary to accommodate shrinkage cannot occur. Finally, it may be speculated that the higher content of oxygen or other impurities in Powder II helps to promote the phase transformation from  $\beta \rightarrow \alpha$  SiC.

### III. Dihedral Angles in Sintered $\beta$ -SiC

On the basis of thermodynamic considerations it has been hypothesized<sup>(6)</sup> that densification can only take place in a sintering solid if the equilibrium dihedral angle ( $\theta$ ) is greater than 60° for a pore surrounded by 3 grains; or that  $\gamma_{GB}/\gamma_{SV}$ , the ratio of the grain boundary to solid-vapor surface energy, be  $< \sqrt{3}$ . These parameters are interrelated by Young's equation

$$\gamma_{GB} = 2\gamma_{SV} \cos \frac{\theta}{2}. \quad (3)$$

Transmission electron and scanning electron microscopy were employed to observe dihedral angles in  $\beta$ -SiC containing carbon, boron and carbon, and only boron. Three sample preparation techniques were used to help reveal grain boundary-solid vapor intersections in these materials. In the case of TEM studies, 1) sintered powders were ultrasonically dispersed, placed on carbon substrates and then photographed by electron transmission or 2) sintered samples were thinned in an ion micromilling apparatus and then examined by direct electron transmission. SEM was used to observe fractured surfaces of sintered compacts.

A large number of dihedral angles were observed in the photographs shown in Figs. 8-13. Photomicrographs of sintered particles of  $\beta$ -SiC + 0.8% C shown in Figs. 8 and 9 reveal that all dihedral angles observed appear to be larger than  $100^\circ$ . A pore surrounded by 5 grains in a sintered compact of this material is shown in Fig. 10. Again, the dihedral angles appear to have values near  $100^\circ$ . Figure 11 is a SEM photomicrograph of the same powder which was first hot-pressed to 79% of theoretical density at  $2050^\circ\text{C}$  at 10,000 psi for 1 hr and then sintered at  $1900^\circ\text{C}$  for 2 hrs without any further change in density. Note that nearly all dihedral angles are well over  $100^\circ$ . Because these dihedral angles are much higher than the critical angle of  $\sim 60^\circ$ , this powder should have no thermodynamic limitations on densifying during sintering. However, it is observed experimentally that this powder will not densify to any extent even when heated to temperatures  $\sim 2100^\circ\text{C}$ .

Boron-doped  $\beta$ -SiC powder (S.A.  $\sim 8-10 \text{ m}^2/\text{g}$ ), likewise, does not densify more than 1% even at very high temperatures. Inspection of the neck regions between sintered particles shows that the dihedral angles are also more than  $100^\circ$  (see Fig. 12). Similar large dihedral angles are observed in highly sinterable powders, such as Powder I,



Fig. 8 TEM photomicrograph of sintered particles of loose powder of  $\beta$ -SiC containing 0.8% C fired at 1900°C for 1 hr in argon. 40,000X



Fig. 9 TEM photograph of a group of sintered particles of  $\beta$ -SiC. Sintered at 1900°C for 1 hr in argon. 100,000X



Fig. 10 Five-sided pore in the microstructure of a powder compact of  $\beta$ -SiC containing 0.8% C that was sintered at 1900°C for 1 hr in argon. 150,000X

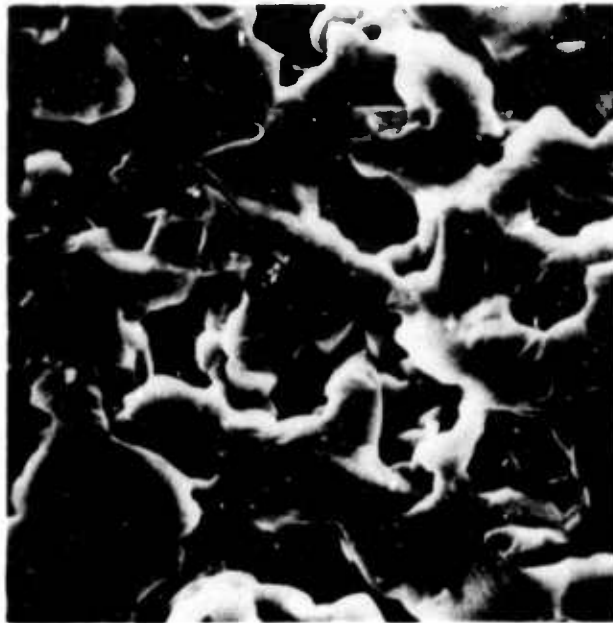


Fig. 11 Microstructure of hot-pressed  $\beta$ -SiC containing 0.8% C which was subsequently annealed at 1900°C for 2 hrs in argon. 2000X



Fig. 12 Sintered particles of loose powder of  $\beta$ -SiC containing 0.6% B  
fired at 1900°C for 2 hrs in argon. 100,000X

which contain both C and B additions. Such a powder is shown in Fig. 13.

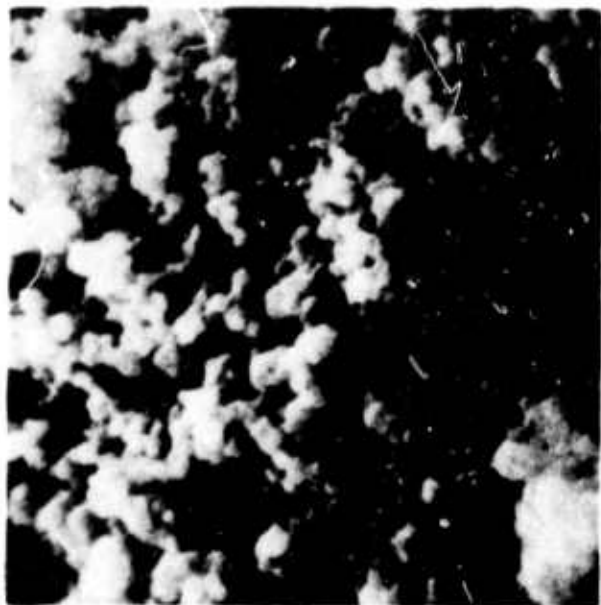
Observations of the dihedral angle at the junction of a grain boundary with the solid-vapor surface of a pore show, therefore, that the dihedral angle is larger than  $100^\circ$  in  $\beta$ -SiC powders that do not densify just as in those that do densify during sintering. It may be that grain boundaries of high energy orientation, which would produce small dihedral angles, are so unstable that they may not form at all. This could also be the reason why small dihedral angles ( $<70^\circ$ ) have not been observed in any microstructure developed in the intermediate stage of sintering.

#### IV. Development and Shrinkage of Grain Boundaries in $\beta$ -SiC Containing 0.8% C

In the first Semi-Annual Technical Report<sup>(1)</sup> the development of microstructure during the early stage sintering of  $\beta$ -SiC powder containing excess carbon was discussed. Compacts of this powder do not exhibit densification at temperatures up to 2100 C in Ar. The microstructure of this material when sintered at 1900 C is shown in Fig. 14 along with that of the unsintered or "green" material. Sintered  $\beta$ -SiC containing excess carbon is seen to be characterized by a highly porous, interconnected structure having randomly distributed, highly dense regions composed of clusters of grains. The average width of the pore spaces between the dense clusters of grains is about  $0.8 \mu$ . This is slightly larger than the average grain size which is about  $0.6 \mu$ . The clusters of grains have an average size of  $\sim 2.5 \mu$  and are larger than the average grain size and pore width. A cluster contains, on the average, about 72 grains, assuming that the grains are spherically shaped. Put another way, the number of original powder particles,  $0.17 \mu$  in average size, required to produce one dense cluster of grains is more than 3,000.



Fig. 13 Sintered particles of loose powder of  $\beta$ -SiC containing 0.8% C and 0.6% B fired at 1900°C for 2 hrs in argon.  
100,000X



A



B

Fig. 14 SEM photomicrograph of a fractured surface of (A) a "green" compact and (B) sintered compact (1900°C-1 hr-Ar) of  $\beta$ -SiC powder containing 0.8% C.

To account for this kind of microstructure, it is postulated that a large number of interparticle contacts either do not develop into grain boundaries or that, once developed, they break; perhaps as a result of local tensile stresses which develop during the early stages of sintering. An experiment done to check this idea was to hot-press some of this same  $\beta$ -SiC powder containing excess carbon in order to force the formation of a large number of grain boundaries per unit volume. The hot-pressed specimen was then annealed without pressure being applied and the changes which occurred in the pore-grain structure observed by SEM.

The photomicrographs in Figs. 15-17 show microstructures of sintered, hot-pressed, and hot-pressed and annealed  $\beta$ -SiC containing 0.8% C. First of all, as a reference structure, Fig. 15 is the microstructure of a powder compact which has only been sintered at 1900°C for 1 hr. The microstructure of a sample hot-pressed at 2050°C for 1 hr at 10,000 psi is shown in Fig. 16. Photomicrographs of the hot-pressed sample which was subsequently annealed at 1700°C and 1900°C are shown in Figs. 17A and 17B, respectively. The sintered sample has a relative density of 59%, the same as that of the original green compact. The hot-pressed sample densified to a relative density of 79%, but the subsequent annealing treatments caused no further change in density to occur. A comparison of grain sizes in the sintered and hot-pressed  $\beta$ -SiC indicates that the hot-pressed specimen has about twice the grain size ( $\sim 1.2 \mu$ ) of the sintered specimen ( $\sim 0.6 \mu$ ). The larger grain size is due to the higher temperature used during hot-pressing (2050 vs. 1900°C).

Annealing the hot-pressed sample at 1700°C causes little change in microstructure except for some smoothing of solid surfaces, probably by surface diffusion. A major transformation in microstructure occurs during annealing at 1900°C for 2 hrs, since an appreciable amount of grain growth and pore growth occur. The resulting microstructure is identical to that of the sintered sample except for

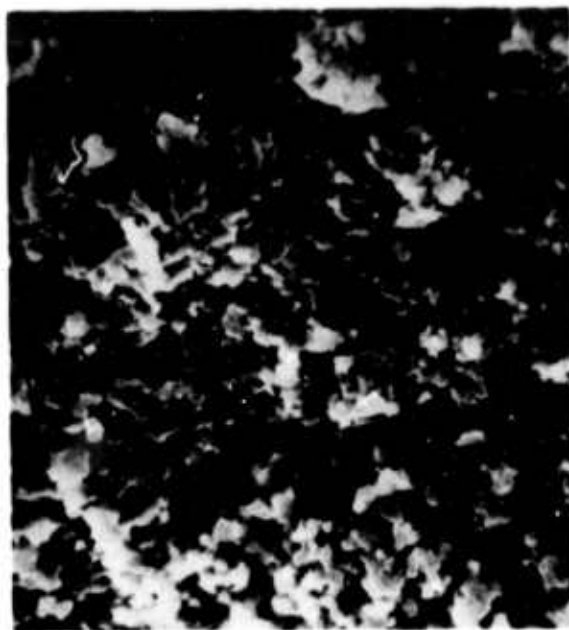


Fig. 15 Microstructure of a sintered specimen of  $\beta$ -SiC containing 0.8% C fired at 1900°C for 1 hr in argon. SEM of fractured surface. 2000X

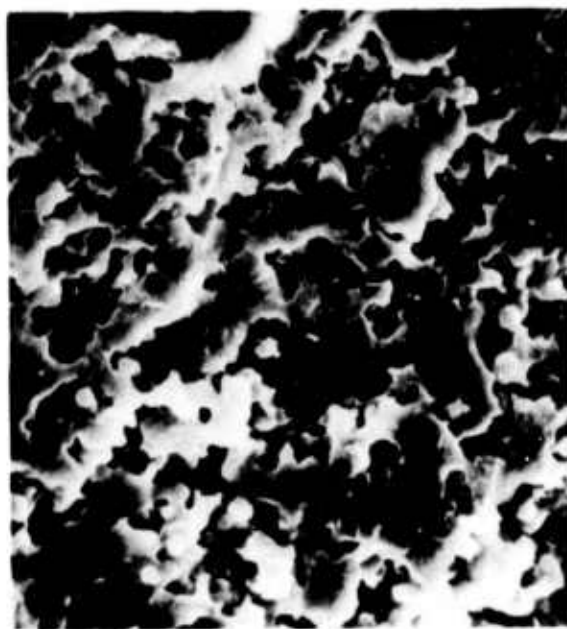
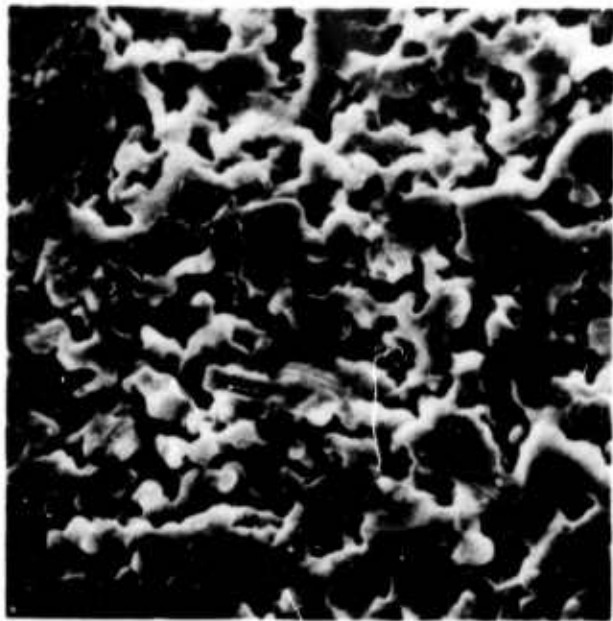
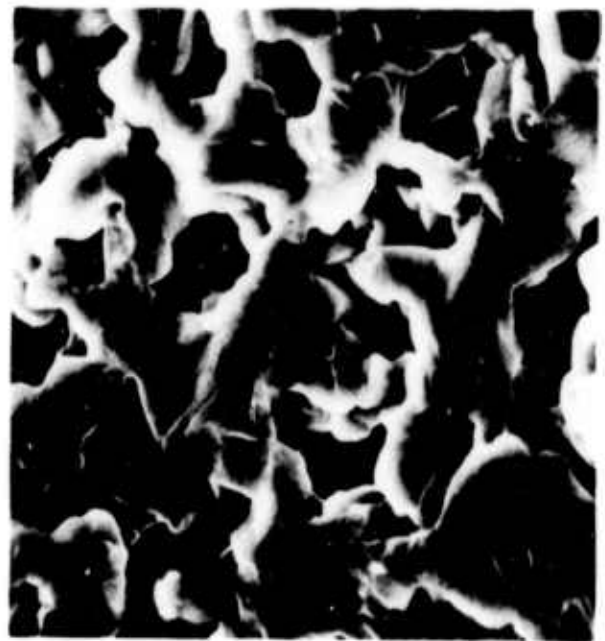


Fig. 16 Microstructure of a hot-pressed specimen of  $\beta$ -SiC powder containing 0.8% C. Specimen was hot-pressed at 10,000 psi for 1 hr at 2050°C. SEM of fractured surface. 2000X



A



B

Fig. 17 Microstructure of hot-pressed  $\beta$ -SiC containing 0.8% C which was (A) annealed at 1700°C and (B) annealed at 1900°C for 2 hrs in argon. SEM of fractured surface. 2000X

a change in scale. Since a major amount of grain and pore growth occur during the 1900°C anneal, a temperature 150°C below the hot-pressing temperature, the microstructure of the hot-pressed sample must be very unstable with respect to thermal treatment at 1900°C in the absence of an applied pressure. The instability in structure is believed to originate from the instability of a large number of high energy grain boundaries which are metastable-to-stable during hot-pressing when compressive forces are applied, but become unstable in the absence of such compressive forces. During subsequent sintering at temperatures where sufficient matter transport can occur, these high energy grain boundaries shrink, thus ultimately breaking the contact between grains within a certain range of mutual orientation. This process is accompanied by high surface diffusion which permits rapid grain growth (coarsening) and pore growth in these porous microstructures. In Figs. 17A and 17B several narrow "necks" or grain boundaries can be seen which may indicate those grain boundaries which are in the process of disappearing.

## V. Sintering of Silicon

### A. Introduction

Silicon is a covalently bonded solid of well known properties which is generally regarded as being unsinterable. It is ideal for the study of sintering in covalent solids because it can be obtained in high purity form and a wealth of information has been accumulated on its physical and chemical properties in single crystal form, including impurity diffusion data. Technologically, sintered silicon could be an important source material for the formation of reaction-bonded  $\text{Si}_3\text{N}_4$ . Furthermore, large complex shapes of theoretically dense, polycrystalline silicon may have potential applications in a variety of electronic applications.

The sintering behaviors of silicon powders are being investigated to determine the characteristics they have in common with those of  $\beta$ -SiC powders. Similar work is in progress on  $\text{Si}_3\text{N}_4$  powders and will be reported at a later time. The studies are aimed at revealing the causes of the normal "unsinterability" of the whole class of powders of covalently bonded solids.

## B. Sintering crystalline silicon powders

### 1. Powder preparation

The silicon used had been purchased from Monsanto Research Corp., St. Peters, Missouri. It is their Hyperpure grade prepared by thermal decomposition of trichlorosilane and is used for manufacturing semiconductors. It was obtained in the form of polycrystalline chunks about 1" in diameter which were broken pieces of a rod pulled from a melt. The minimum resistivity of the silicon was 100 ohm-cm which indicated a total impurity content of less than about 2 ppb. The chunks were crushed with a mortar and pestle of high purity copper. The resulting powder was sieved through brass screens and then leached in aqua regia for 24 hours to dissolve any metal. The acid was changed after the first 4 hrs. After leaching, the powder was washed thoroughly with distilled water and dried.

Fine particles of silicon in the micron-to-submicron size range were prepared by feeding -325 mesh silicon particles into a Trost fluid energy (jet) mill. This type of milling device has the significant advantage of producing fine powder with control of particle size and distribution while maintaining purity. This mill functions by making use of compressed air to carry the particles to be broken. This is expanded through two diametrically opposed jets to achieve high relative velocities of the particles so that fracture by mutual impact can occur. The fractured particles are then passed through a classifier, and the fines collected. The structure of the collection system permitted silicon powders with an average particle size of

1.35  $\mu$  and 0.23  $\mu$  to be collected in different regions. These average particle sizes were determined from surface area measurements made by the B.E.T. method using flowing 30% N<sub>2</sub> in He.

Chemical additions of 0.2 wt% C and 0.2 wt% C + 1.2% B were introduced into each of the fine silicon powders in order to determine the effect of composition on densification. The type of carbon used was Cabot Monarch 71 which has an average particle size of 160 Å. Elemental boron was purchased from Callary Chemical Co. and had an average particle size of 350 Å. The desired compositions were mixed for 1 hr in a Spex Industries Mixer/Mill (Model 8000-11) using acetone as a dispersing medium.

Carbon was selected because it could enhance the removal of SiO<sub>2</sub> layers on the Si particles by chemical reduction and, consequently, maintain a high surface energy of Si, which drives the sintering process. Boron was selected as an additive because it has limited solid solubility in Si and may act as a grain growth inhibitor during sintering in the same way that B, MgO and ThO<sub>2</sub> affect grain growth and sintering in  $\beta$ -SiC, Al<sub>2</sub>O<sub>3</sub> and Y<sub>2</sub>O<sub>3</sub>, respectively.

## 2. Sintering experiments and results

Sintering experiments were performed on powder compacts (5/8" diameter  $\times$  1/4" thick) of each composition which had been fabricated by isostatic pressing at 30,000 psi. The green density of nearly all specimens was 56% of theoretical. Each specimen was fired in an open Al<sub>2</sub>O<sub>3</sub>-boat placed inside an Al<sub>2</sub>O<sub>3</sub> tube, closed on one end, located inside a Pt-Pt 40% Rh wound resistance furnace. In all cases, the prevailing atmosphere was flowing argon at 2 SCFPH which is first passed through an "oxygen gettering" furnace before entering into the sintering furnace. The partial pressure of oxygen in the sintering furnace is estimated to be  $\sim 10^{-8}$  atm.

The effect of particle size and composition on the fired density of silicon is shown in Table III. The pure, crystalline silicon powder

TABLE III

Effect of Particle Size and Composition on Density  
of Silicon Sintered at 1350°C for 1 hr in Ar

<u>Powder</u>	<u>Composition</u>	<u>D<sub>o</sub> (g/cc)</u>	<u>D (g/cc)</u>	<u><math>\frac{\Delta L}{L_o}</math> (%)</u>
Powder A (1.3)	Si	1.28	1.325	1
"	Si+0.2 wt% C	1.30	1.30	0
"	Si+0.2 wt% C+1.2% B	1.31	1.35	1.5
Powder B (0.23)	Si	1.26	1.36	2.4
"	Si+0.2 wt% C	1.27	1.32	1.3
"	Si+0.2 wt% C+1.2% B	1.28	1.43	4

$D_o$  = density of green compact

D = fired density

$\frac{\Delta L}{L_o}$  = linear shrinkage

densifies only a few percent when sintered at 1350°C, a temperature which is about 96% of the melting point. By using an average particle size of 0.23  $\mu$  instead of 1.3  $\mu$ , the linear shrinkage increases from 1 to 2.4%. The addition of a small amount of carbon actually decreases the amount of shrinkage from 1 to ~0% in Powder A; this shrinkage reduction possibly being due to the formation of SiC during sintering. The fired sample did have some strength, indicating that interparticle necks formed. The addition of both boron and carbon to Powder A and Powder B does increase the shrinkage and fired density. There is little change in the amount of densification when the doped or undoped Si powders are sintered at temperatures higher than 1350°C but below a temperature at which any liquid forms. However, Powder B, which contains 0.2% C + 1.2% B, was sintered to greater than 99% of theoretical density at 1391  $\pm$  2°C, a temperature slightly above the eutectic temperature. Considerable densification can, therefore, be achieved by the presence of eutectic liquid. A polished section of the dense, sintered sample, illustrated in Fig. 18, shows 1) a small percentage of large, porous second phase particles (dark grey) which are probably SiC, 2) a large fraction of fine micron-size particles (light grey) which are B<sub>4</sub>Si (identified X-ray diffraction) and 3) a few small pores (black spots) about 5  $\mu$  in size.

In an attempt to determine if the densification of Si in the solid state is limited by the presence of a SiO<sub>2</sub> layer on the surfaces of the particles, a chemical leaching experiment was done by soaking 0.23  $\mu$  Si powder for 1 hr in HF. A rapid reaction occurred as evidenced by froth formation on the surface of the stirred suspension. The powder was washed, filtered, dried, compacted and then sintered at 1350°C for 1 hr in argon. Again, the sample had the same fired density as that prepared from unleached powder. This experiment suggests silicon oxide surface layers are not totally responsible for the limited densification of submicron silicon powder during sintering.

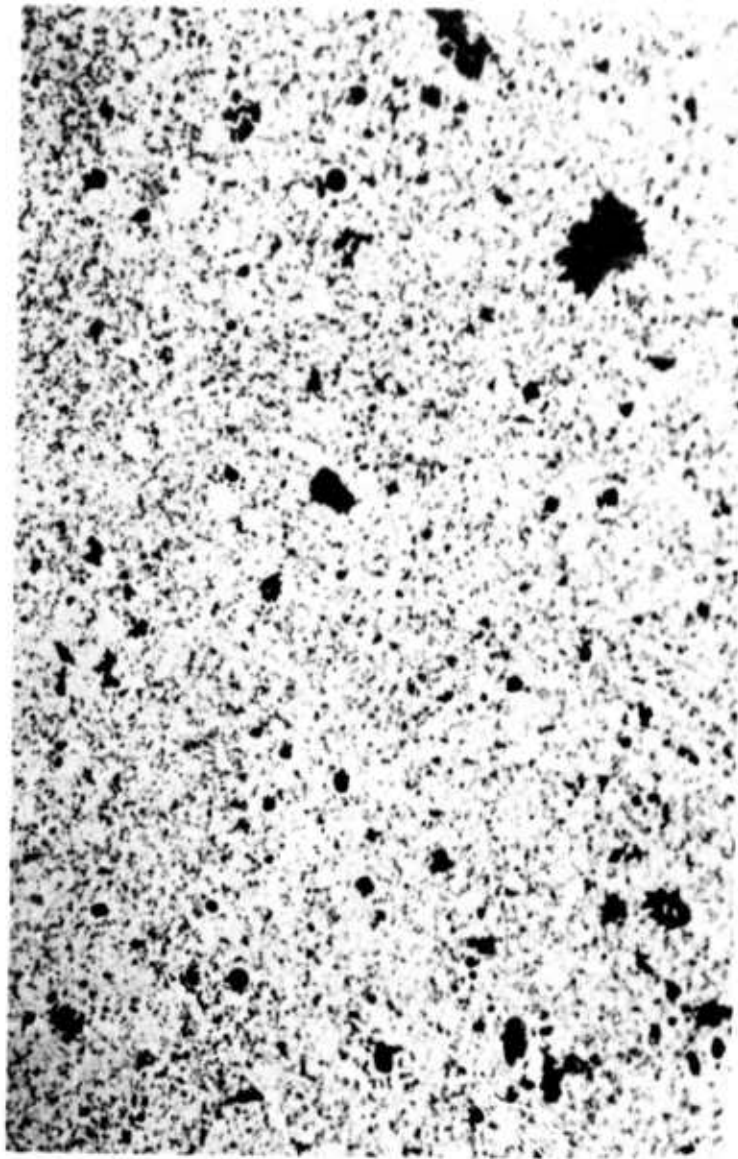
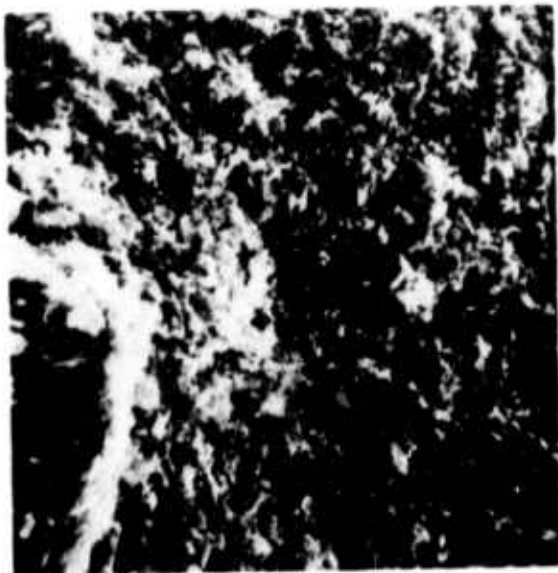


Fig. 18 Microstructure of silicon containing 0.2% C and 1.2% B sintered to 99+% of theoretical density at 1391°C for 1 hr in argon. Reflected light photomicrograph of polished section. 500X

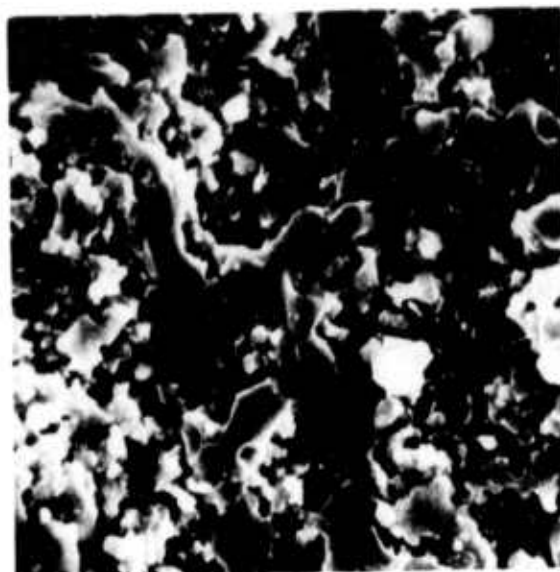
### 3. Observations on microstructure

The effects of heat treatment and composition on the microstructure of sintered silicon are shown in Fig. 19. The results of sintering Powder B ( $0.23 \mu$ ) have been chosen for representation and are identical in detail to those of Powder A except for a change in scale. Sintered silicon has a microstructure (Fig. 19B) characterized by interconnected pores and interconnected solid in which considerable grain and pore growth have taken place (compare Figs. 19A and 19B). The microstructure of sintered silicon is identical to that previously found for sintered  $\beta$ -SiC containing excess carbon. This is readily apparent when comparing Fig. 20 (a higher magnification of Fig. 19B) with Fig. 14B. Large, pore-free solid regions and large pores are evident in the microstructure of sintered silicon shown in Fig. 20. The dense solid regions have an average size of about  $4 \mu$  and have the volume of more than 5,000 of the initial powder particles. In addition, the fine pore space originally located between the initial powder particles has been relocated into large pores surrounding the dense solid regions. A polished and chemically etched section of sintered silicon (Fig. 21) reveals that these dense solid regions are polycrystalline. This information can help lead to an understanding of the development of this type of structure.

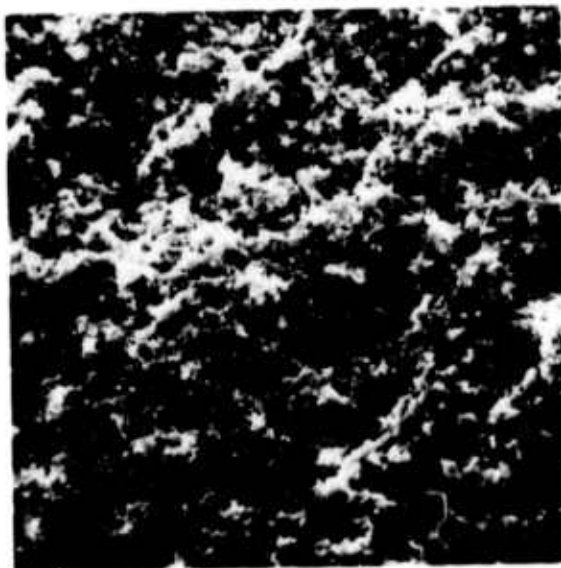
Addition of carbon and boron to silicon produces a remarkable change in the microstructure of the sintered body (Fig. 19C). These additions act to generate a fine grain-fine pore structure which permits a greater amount of densification during sintering. These two additions cause the same type of microstructure to develop in  $\beta$ -SiC, except that  $\beta$ -SiC powder containing 0.6% B + 0.8% C densifies up to 96% of theoretical density whereas Si powder containing 1.2% B + 0.2% C densifies only to about 62% of theoretical density. Lattice parameter measurements on sintered samples of boron-doped  $\beta$ -SiC and Si show that the lattice parameter decreases from its value for the pure material, indicating that boron goes into solid solution in both materials.



A



B



C

Fig. 19 SEM photomicrographs of fractured surfaces of (A) a green compact of silicon before sintering, (B) a sintered compact of silicon, and (C) a sintered compact of silicon containing 0.2% C and 1.2% B. Specimens (B) and (C) were sintered at 1350°C for 1 hr in Ar. 1000X

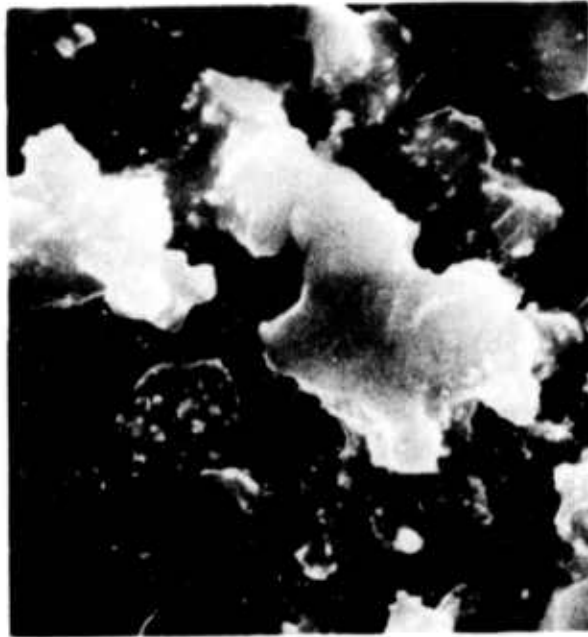


Fig. 20 SEM photomicrograph of a fractured surface of silicon  
sintered at 1350°C for 1 hr in Ar. 5000X

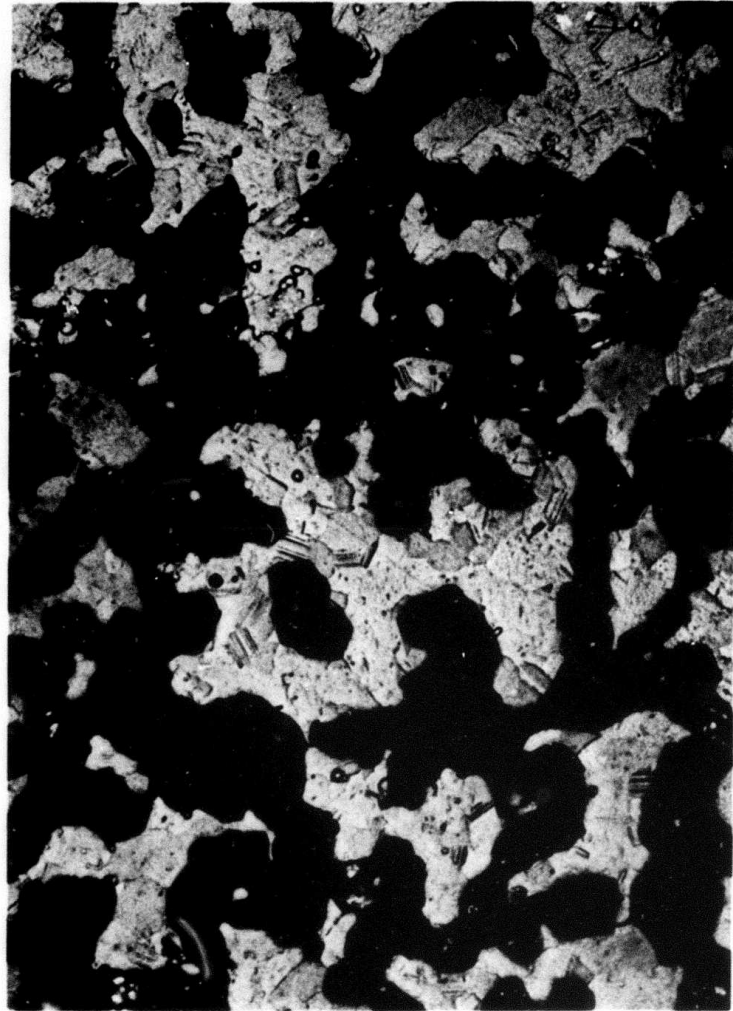


Fig. 21 Reflected light micrograph showing polycrystalline nature of the solid, dense regions developed during the sintering of silicon at 1350°C for 1 hr in Ar. Polished section was chemically etched with mixture of equal parts of HF and HNO<sub>3</sub> at room temperature for 2 seconds.

### C. Preparation and sintering of amorphous silicon powders

It is desirable to study the effect of average particle sizes less than  $0.2 \mu$  and degree of crystallinity on the densification behavior of pure silicon powders during solid-state sintering. Since to our knowledge, such fine Si powders with high purity are not commercially available, it was decided to prepare our own material.

Silicon powder was prepared by the thermal decomposition of silane,  $\text{SiH}_4$ , between 600 and  $700^\circ\text{C}$  in a gradient furnace. The following reaction takes place:



The source of silane was a 4% silane + 96% helium "calibration mixture" produced by the Linde Division of Union Carbide. This gaseous mixture flowed into a fused silica tube located inside the furnace. The silicon powder (or smoke) deposited on the inner wall of the tube. The powder was scraped from the glass wall and characterized by X-ray diffraction, surface area measurements and sintering experiments.

Two experimental runs were made, and powders prepared from these runs are designated Si-1 and Si-2. Si-1 powder was prepared by using a gas flow rate of 0.5 SCFPH and a maximum furnace temperature of  $700^\circ\text{C}$ . Si-2 powder was prepared with a gas flow rate of 2 SCFPH and a maximum furnace temperature of  $650^\circ\text{C}$ . The color of Si-1 powder was dark brown. Si-2 powder was inhomogeneously brownish-grey in color. Since the powders were prepared in a temperature gradient furnace, these powders are probably inhomogeneous with respect to particle size, morphology and crystallinity. Therefore, both powders were given an isothermal anneal at  $700^\circ\text{C}$  in flowing Ar. After the annealing treatment the color of the Si-1 powder turned light brown while that of Si-2 powder turned dark brown to yellowish brown. X-ray diffraction

analysis of these powders showed that Si-1 powder was amorphous in the "as-prepared" form but partly crystallized after the isothermal anneal at 700°C. Preliminary X-ray results on Si-2 powder show it to be partly crystalline in the "as-prepared" state but highly crystallized after the isothermal treatment at 700°C.

Preliminary results of the sintering behavior of these submicron silicon powders are shown in Table IV. An exciting discovery was that Si-1 powder, having a specific surface area of 44 m<sup>2</sup>/g (corresponding to 585 Å particles), sintered to 92.3% of theoretical density at 1350°C. It is believed that at temperatures between 1350 and 1410°C (the melting point of Si) this powder will sinter to nearly theoretical density. This finding is highly encouraging for it engenders hope that other "pure" covalent solids can be sintered to densities greater than 90% of theoretical.

Si-2 powder, which has a specific surface area of ~14.5 m<sup>2</sup>/g (~1760 Å particles), densifies only to a limited extent and shrinks not more than 8% at 1350°C. These sintering results on silicon appear to indicate the extreme importance of starting with a powder of high surface area to obtain high densification of "pure" covalent materials. The results also imply that shrinkage during sintering increases with increasing amorphism of the starting silicon powder. This can be seen from the results listed in Table V which summarizes the methods of preparation of highly pure silicon powder state of crystallinity and specific surface area, and the amount of linear shrinkage under constant sintering conditions.

Finally, an interesting experimental correlation between percent linear shrinkage and specific surface area of the various silicon powders is illustrated in Fig. 22. There appears to be an approximately linear relationship between these two parameters. Three of the data points fit on a straight line which passes through the origin. One data point falls well off this line. Such a linear relationship can be predicted from sintering theory if the starting powder compacts

TABLE IV  
Specific Surface Area and Sintered Densities  
of Silicon Powders Prepared from Silane

<u>Powder</u>	<u>S.A. (m<sup>2</sup>/g)</u>	<u>Sintering conditions</u>	<u>D<sub>o</sub> (%)</u>	<u>D (%)</u>	<u><math>\frac{\Delta L}{L_o}</math> (%)</u>
Si-1, annealed at 700°C	44	1350°C-1 hr	43	92.3	23
Si-2, as prepared	14.6	"	48	61	8
Si-2, annealed at 700°C	14.4	"	48	56	5

---

S.A. = specific surface area

D<sub>o</sub> = green density of compact

D = fired density

$\frac{\Delta L}{L_o}$  = linear shrinkage

TABLE V

Powder Characteristics and Sintering Behavior of Silicon

<u>Method of preparation</u>	<u>State of crystallinity</u>	<u>S.A. (m<sup>2</sup>/g)</u>	<u>Heat treatment</u>	<u><math>\frac{\Delta L}{L_0}</math>(%)</u>
Jet milling	crystalline	1.9	1350°C-1 hr-Ar	1
"	crystalline	11.4	"	2.5
Decomposition of silane	partly amorphous	14.6	"	8
"	amorphous	44	"	23

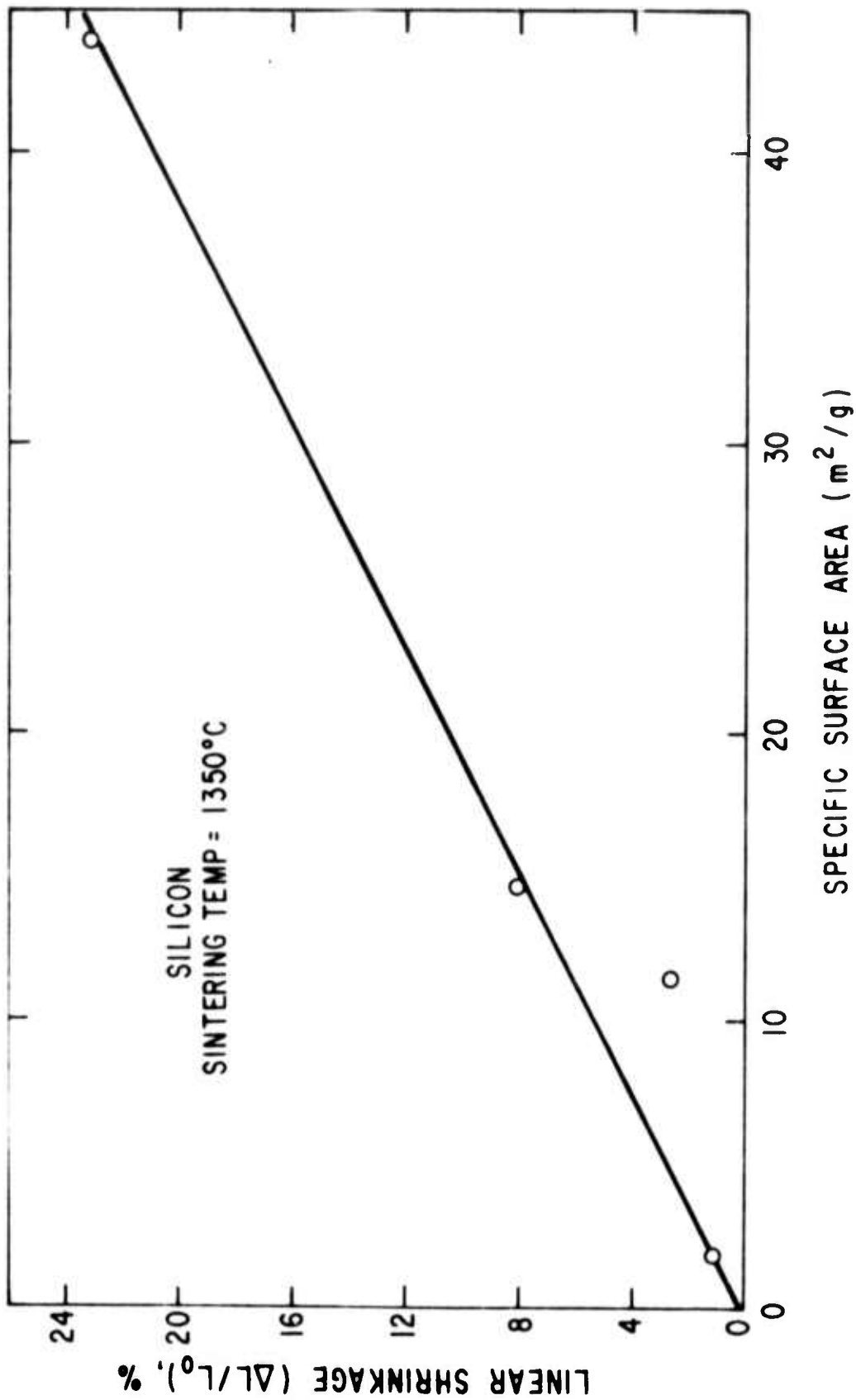


Fig. 22 Linear shrinkage as a function of specific surface area for silicon powders sintered at 1350°C for 1 hr in Ar.

have a narrow range of green densities and if the pore-grain geometry is such that all pores form an interconnected structure and are intersected by grain boundaries during sintering. From early stage sintering theory  $\Delta L/L_0$  is approximately inversely proportional to  $1/r$ , where  $r$  is the average particle size. Because  $1/r$  is directly proportional to specific surface area, S.A., a simple linear relationship between  $\Delta L/L_0$  and S.A. is predicted.

## VI. Properties of Doped, Dense, Sintered SiC

### A. Resistivity

The high temperature stability of 98+% dense, sintered  $\beta$ -SiC coupled with the known electrical properties of single crystals leads to an anticipation that sintered  $\beta$ -SiC might find some unique applications in electrical components. In order to assess this possibility, basic information on electrical properties of sintered  $\beta$ -SiC is needed. The task of this study was to determine whether the electrical conductivity of sintered  $\beta$ -SiC would be affected by dopants in a manner similar to that of  $\beta$ -SiC single crystals. Uncertainty about this arises from the fact that sintered  $\beta$ -SiC always contains boron, which is a necessary sintering additive, at a level (up to 0.4 wt%) which might totally dominate the electrical behavior.

The semiconductive nature of  $\beta$ -SiC has been extensively studied on single crystals, and is described in works by Busch<sup>(7)</sup>, Lely and Kröger<sup>(8)</sup>, Van Daal, et al<sup>(9)</sup>, Bathe and Hardy<sup>(10)</sup>, and the review by Neuberger<sup>(11)</sup>. Briefly, atoms of the fifth group (nitrogen and phosphorous) introduce donor levels 0.06 to 0.08 eV below the conduction band which are excited at low temperature and produce conductivity ( $10^3$ - $10^9$  ohm<sup>-1</sup>cm<sup>-1</sup> at RT). Trivalent atoms (B and Al) form acceptor levels about 0.28 to 0.35 eV above the valence band which are little excited at room temperature.

Thus, B and Al doping results in much lower conductivity ( $10^{-2}$ - $10^{-5}$  ohm $^{-1}$ cm $^{-1}$ ). In reality, this simple model is rarely applicable because complicating effects arise from other levels almost always present, but whose origin has not yet been identified, from interaction of donors and acceptors, from exhaustion of some donor or acceptors at higher temperature, from degeneracy at high concentrations of dopants, etc.

Previous work done with boron-doped hot-pressed  $\beta$ -SiC<sup>(12)</sup> has shown that the effect of boron (as an acceptor forming dopant) can indeed be compensated by nitrogen if a sufficient amount of it has been introduced in the form of silicon nitride. A Si<sub>3</sub>N<sub>4</sub> addition thus resulted in n-type behavior in hot-pressed  $\beta$ -SiC which exhibited room temperature conductivity on the order of 1 to 5 ohm $^{-1}$ cm $^{-1}$ .

Similar results were obtained in the investigation of sintered, boron-doped  $\beta$ -SiC when sintering was done in an atmosphere containing nitrogen. However, since nitrogen retards densification<sup>(13)</sup>, the sintering temperature has to be increased in order to achieve full densification. The nitrogen partial pressure was set by controlling argon and nitrogen flow (pure "tank quality" gasses, less than 10 ppm oxygen according to the supplier) through the carbon resistor sintering furnace. The data on the effect of nitrogen in the sintering atmosphere on the room temperature resistivity of boron-doped,  $\beta$ -SiC are summarized in Table VI, along with data for boron-doped  $\beta$ -SiC sintered in argon.

Resistance was measured with an electronic voltmeter at 6 V DC and 150 AC (with identical results) on 12 mm diameter, 6 mm thick pellets with 6 mm diameter aluminum electrodes sputtered on ground faces.

Boron-doped  $\beta$ -SiC sintered in absence of nitrogen or at a low pressure of N<sub>2</sub> exhibits substantial variation in resistivity. Values between  $10^2$  to  $10^4$  (Table I) were observed. The origin of this

TABLE VI

Effect of Sintering Furnace Atmosphere on the Resistivity of B-doped, Dense, Sintered  $\beta$ -SiC

Starting powder Code	%B addition	Sintering atmosphere & pressure (torr)	Sintering temperature (°C)	N <sub>2</sub> % by vac. fusion	Resistivity RT (ohm-cm)	Remark
ES-11	.5	1 Ar	1950	n.d.	$1.7 \times 10^2$	hot-pressed
146-1989	.36	760 Ar	2080	<0.005	$1.2 \times 10^3$	
146-2056	.4	0.2 Ar	2080	n.d.	$8.0 \times 10^3$	acid leached powder
146-1989	.36	50 N <sub>2</sub>	2100	n.d.	$1.6 \times 10^3$	
146-1989	.36	100 N <sub>2</sub>	2190	n.d.	$3.3 \times 10^2$	
146-1989	.36	450 N <sub>2</sub>	2280	0.41	0.32	
146-1989	.36	760 N <sub>2</sub>	2300	n.d.	0.51	
146-1893	.9	760 N <sub>2</sub>	2180	n.d.	0.80	
146-1989	.36	760 Ar	2050	n.d.	$4 \times 10$	1.0% Be <sub>2</sub> C

variability is not presently known. The observation that sintering in vacuum tends to increase the resistance suggests that it may be related to furnace atmosphere contaminant such as aluminum or oxygen.

The effect of nitrogen is probably first noticeable at a partial pressure of 100 torr. Further increase in  $P_{N_2}$  to 650 torr brings about a drop of three orders of magnitude in resistivity and an unexpectedly high nitrogen content in the sintered body (0.41%  $N_2$ ).

Investigation of the effect of other dopants is in progress. An interesting preliminary result has been obtained from samples of  $\beta$ -SiC doped with beryllium in the form of a  $Be_2C$  addition (Table 1). This dopant increases low temperature conductivity, but does not measurably affect that at high temperature.

Figure 23 shows resistivity vs.  $1/T$  plots for  $\beta$ -SiC that had been boron-doped and: 1) hot-pressed; 2) sintered; 3) nitrogen-doped and hot-pressed; 4) beryllium-doped and sintered. All measurements were made on  $4 \times 1.5 \times 25$  mm bars with sputtered gold electrodes by a four contact technique at 6 V DC. The activation energies calculated for the boron-doped specimens between room temperature and  $600^\circ C$  were 0.27 and 0.285 eV; values essentially identical to those found for boron-doped SiC single crystals<sup>(8)</sup>. The beryllium/boron-doped specimen tends to have a similar activation energy at elevated temperatures. Specimen 3, heavily doped with nitrogen during hot-pressing, shows little change in resistance between room temperature and  $350^\circ C$  and a large increase above  $350^\circ C$ . Similar behavior has been reported for nitrogen-doped  $\beta$ -SiC single crystals<sup>(8)</sup>, however, in the present case, the polycrystalline material has a much higher positive temperature coefficient.

#### B. Thermal EMF

The thermoelectric EMF of a thermocouple made of nitrogen-doped  $\beta$ -SiC vs. boron/beryllium-doped  $\beta$ -SiC (i.e. of a p-n junction) was measured. For this purpose, circular rods of SiC about  $13 \text{ cm} \times 6 \text{ mm}$

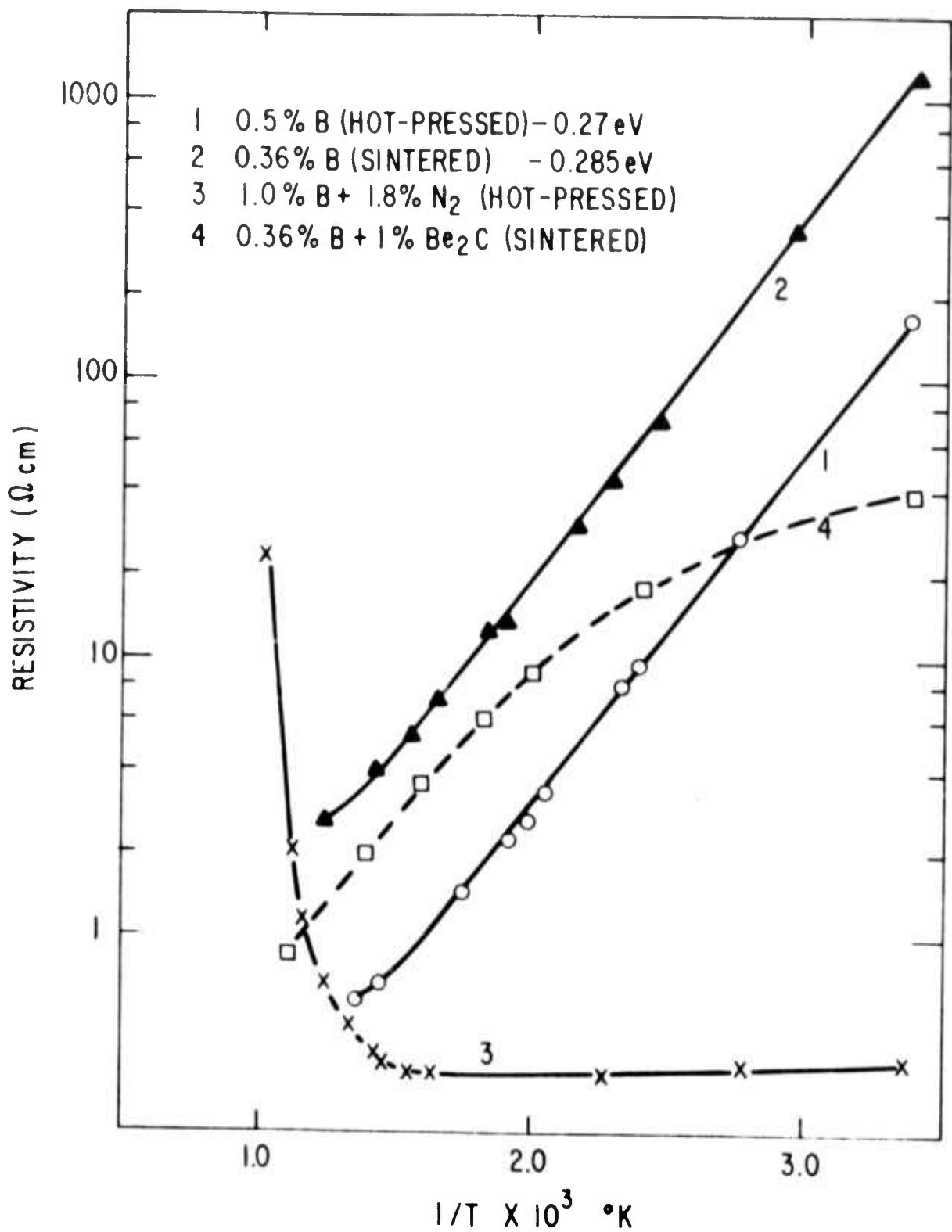


Fig. 23 Resistivity versus  $1/T$  for variously doped hot-pressed, and sintered specimen of  $\beta$ -SiC.

were isostatically pressed and sintered. The couple was made by "soldering" the sintered rods with silicon into two holes drilled into the side of a short carbon cylinder. The other ends of the rods were copper plated to obtain good contact to wires. The junction was inserted into a platinum wound furnace containing a nitrogen atmosphere and the cold ends were kept at boiling water temperature by inserting them into short, water-filled test tubes. The measurements were taken with an electronic voltmeter with an infinite internal resistance both on heating to 1500°C and on cooling. The resistance of the couple was 480 r. Another measurement at low temperature was made with the "cold ends" in an ice bath at 0°C by heating the junction from room temperature to 300°C. The results of both runs are shown in Fig. 24 in terms of EMF vs. temperature difference.

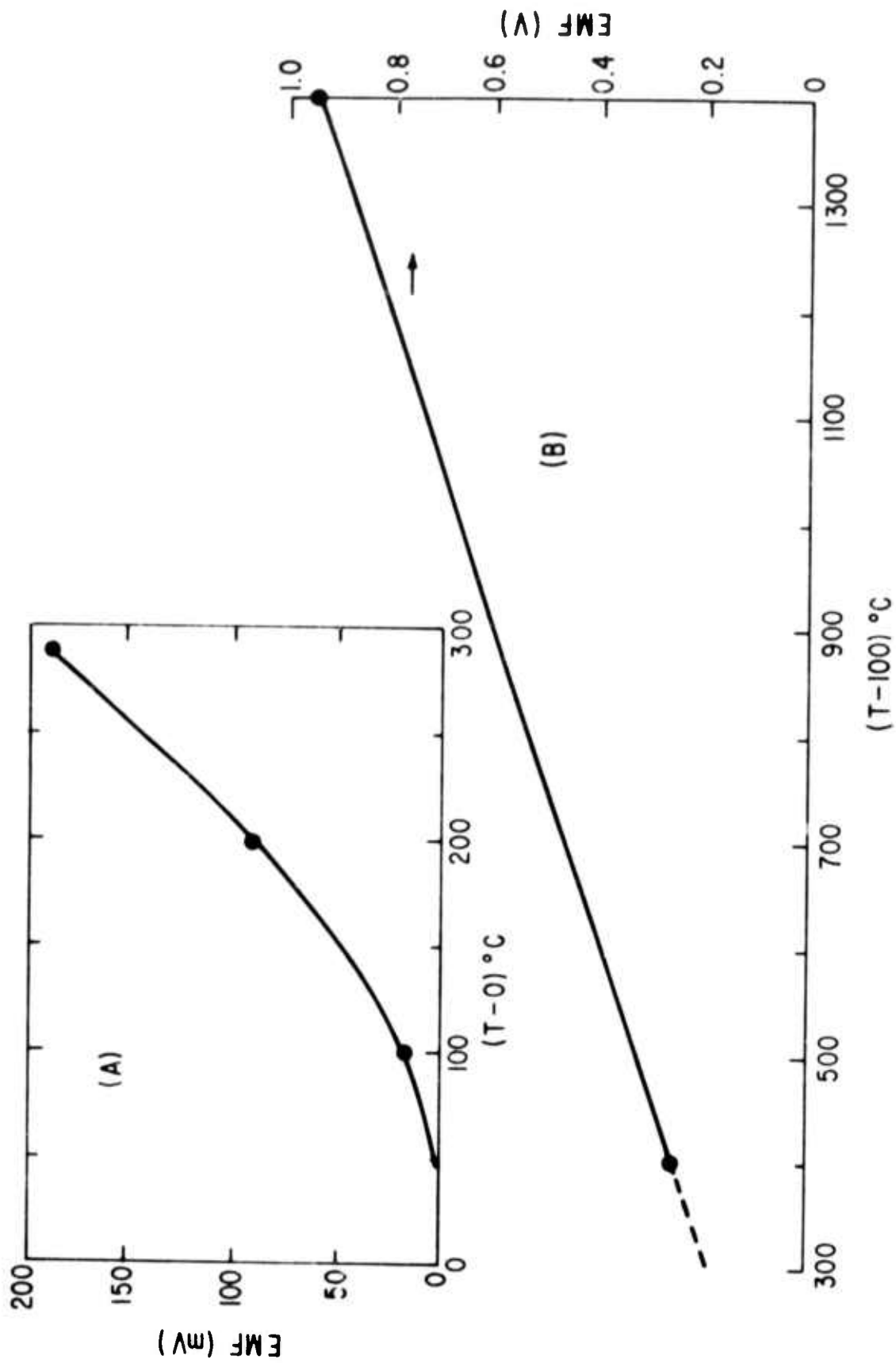


Fig. 24 Thermal EMF of a junction of p and n types of  $\beta$ -SiC for: (A) cold junction at  $0^\circ\text{C}$ , and (B) cold junction at  $100^\circ\text{C}$ .

#### REFERENCES

1. J. H. Rosolowski and C. D. Greskovich, "Ceramic Sintering", Semi-Annual Technical Report, Contract No. N00014-74-C-0331; SRD-74-116, October 1974.
2. J. H. Rosolowski and C. D. Greskovich, J. Am. Ceram. Soc., to be published, May 1975.
3. A. Kuper, H. Letaw, L. Slifkin, E. Sonder and C. T. Tomizuka, "Self-Diffusion in Copper", Phys. Rev. 96(5) 1224-25 (1954).
4. R. L. Coble, "Sintering Crystalline Solids. II. Experimental Test of Diffusion Models in Powder Compacts", J. Appl. Phys. 32(5) 793-99 (1961).
5. T. E. Clare, "Sintering Kinetics of Beryllia", J. Am. Ceram. Soc. 49(3) 159-65 (1966).
6. S. Prochazka, "The Role of Boron and Carbon in the Sintering of Silicon Carbide", G.E. Report No. 74CRD186, August 1974.
7. G. Bush and H. Labhart, "Über den Mechanismus der Elektrischen Leitfähigkeit des Silicium Carbids", Helv. Phys. Acta 19 463 (1946).
8. J. A. Lely and F. A. Kroger, "Electrical Properties of 6H-SiC Doped with N, B or Al" in Halbleiter und Phosphore (1958), p. 525.
9. H. J. van Daal, C. A. A. J. Greebe, W. F. Knippenberg and H. J. Vink, "Investigations on Silicon Carbide", J. Appl. Phys. 32 2225-33 (1961).
10. H. D. Batha and L. H. Hardy, in Silicon Carbide-1973. R. C. Marshall et al eds., University Press, S.C., 1974.
11. Handbook of Electronic Materials, Vol. 5, Plenum Press (1971) p. 56.

(REFERENCES - cont.)

12. S. Prochazka and P. C. Smith, "Investigation of Ceramics for High-Temperature Turbine Vanes", Final Report, Contract No. N62269-73-C-0356; SRD-74-040, April 1974.
13. S. Prochazka, C. A. Johnson and R. A. Giddings, "Investigation of Ceramics for High-Temperature Turbine Components", Quarterly Progress Report No. 2, Contract No. N62269-75-C-0122, April 1975.